

CrystEngComm

Accepted Manuscript



This is an *Accepted Manuscript*, which has been through the Royal Society of Chemistry peer review process and has been accepted for publication.

Accepted Manuscripts are published online shortly after acceptance, before technical editing, formatting and proof reading. Using this free service, authors can make their results available to the community, in citable form, before we publish the edited article. We will replace this *Accepted Manuscript* with the edited and formatted *Advance Article* as soon as it is available.

You can find more information about *Accepted Manuscripts* in the [Information for Authors](#).

Please note that technical editing may introduce minor changes to the text and/or graphics, which may alter content. The journal's standard [Terms & Conditions](#) and the [Ethical guidelines](#) still apply. In no event shall the Royal Society of Chemistry be held responsible for any errors or omissions in this *Accepted Manuscript* or any consequences arising from the use of any information it contains.

ARTICLE

Solvent-controlled 3D Lanthanide-Polyoxometalate Frameworks: Reduction and Stabilization of Ag Nanocomposites and Catalytic Properties

Cite this: DOI: 10.1039/x0xx00000x

Received 00th January 2012,
Accepted 00th January 2012

DOI: 10.1039/x0xx00000x

www.rsc.org/

Guang-Gang Gao,^{a,c} Chao-Yu Song,^a Xi-Ming Zong,^a Dong-Feng Chai,^a Hong Liu^{*a}, Yu-Long Zou,^a Jian-Xun Liu,^a and Yun-Feng Qiu^{*b}

Four three-dimensional lanthanide-polyoxometalate complexes, $[K_4Ln_3(H_2IDC)_3(HIDC)_3(H_2O)_3(SiW_{12}O_{40})] \cdot nH_2O$ ($Ln = La$ (1), $n = 7$ and Ce (2), $n = 6$; $H_3IDC = 4,5$ -imidazolecarboxylic acid) and $[Ln_4(HIDC)_4(H_2O)_8(SiW_{12}O_{40})] \cdot 11H_2O$ ($Ln = La$ (3) and Ce (4)), have been synthesized by solvothermal reactions. Compounds 1 and 2 are 3D architectures including 2D layered structures connected by K^+ cations, which was realized by tuning the reaction media with different ratio of water and ethanol. By comparison, in the cases of 3 and 4, lanthanide ions coordinate to tridentate HIDC ligands forming 2D Ln-organic networks, which are further pillared by α -Keggin type $[SiW_{12}O_{40}]^{4-}$ polyoxoanions and thus constructing new 3D frameworks featuring with 1D channels along a and b axes. All of these complexes could induce the formation of Ag nanocomposites possessing high catalytic activity towards the reduction of 4-nitrophenol (4-NP) in the presence of $NaBH_4$.

Introduction

Polyoxometalates (POMs), as a unique class of fascinating metal oxygen clusters of early transition metals, have attracted extensive attention for many years, due to their intriguing structures and remarkable potential applications in catalysis, electrochemistry, and medicine.¹⁻¹¹ Among wide variety of POMs, the Keggin series has been the most studied. These complexes have the general formula $\{XM_{12}O_{40}\}$, where X is the central atom ($X = Si^{4+}$, P^{5+} , As^{5+} , etc.) and M is a metal in a high oxidation state ($M = W^{5+/6+}$, $Mo^{5+/6+}$, $V^{4+/5+}$, etc.). To render the intrinsic properties of POM, various POMs-transition-metal compounds have been found during the past years,^{9, 12-18} while the reported polyoxometalate-lanthanide-organic hybrids are still limited. To the best of our knowledge, Ln ions are often utilized as versatile connectors in the construction of coordination polymers and their coordination numbers can range from 6 to 12, giving rise to various coordination geometries. Also, Ln cations can endow Ln-POMs complexes useful functions such as luminescent, magnetic, and Lewis-acid catalytic centers.¹⁹⁻²³ However, the rational design and construction of POMs-Ln-organic complex remains an arduous task especially for high-dimensional frameworks.

In general, the POMs fragments containing Ln cations have more flexible coordination patterns than those of common POMs, which allow the formation of higher coordination numbers and have potential to be excellent building blocks to construct 3D architectures. On the other hand, N-heterocycle dicarboxylic acid usually possesses three coordination sites, small volume and versatile coordination behaviors, which has been confirmed to be effective ligand to construct POM-Ln-organic compounds, such as 3D pillar-layered framework,^{24, 25}

3D porous framework,²⁶ and 3D network.^{27, 28} More recently, a sodium-induced 3D compound reported by Zhang *et al.* presents the highest coordinated number of 8 for Preyssel polyoxoanion, which further confirmed that N-heterocycle dicarboxylic acids are effective organic ligands.²⁹ Among the above reported 3D POM-Ln-organic complexes, the number of Ln ions that directly coordinate to polyoxoanion is usually less than 5, especially high-connected Keggin-type polyoxoanion located in POM-Ln-organic complex remains elusive. Furthermore, new synthetic method for obtaining 3D POM-Ln-organic compounds, which possess new structural features and diverse functions, is also an urgent request to pursue by coordination chemists.

Additionally, it should be noted that considerable efforts have been endeavored into the fabrication of novel structures of POM-Ln-organic complexes. However, the utilization of 3D crystals based on POMs is lack of attention in biology, chemistry, and material science.³⁰⁻³² As is known, POMs can undergo reversible multielectron redox transformation while keeping structure intact under certain stimulus, which has been proved in a series of pioneering work.³³ And thus, POMs can also be effective reducing and stabilizing agents for the preparation of noble metal nanocomposites, as confirmed in the past decades.³³⁻³⁶ Very recently, Lan and coworkers reported that Au@IFMC-100 solid has been obtained through spontaneous solid-liquid redox reaction of a POM-based single-crystal tubular compound and $HAuCl_4$, which showed high catalytic activities towards the reduction of $K_3Fe(CN)_6$ and 4-NP.⁹ These results proved that 3D framework based on POMs could be ideal matrix or supports for inducing the growth of

noble metal nanocomposites, and thus render the intrinsic properties of POMs due to synergistic effect with noble nanoparticle.

Inspired by above findings, we herein use Keggin type polyoxometalate, lanthanide salt and 4,5-imidazole dicarboxylic acid (H₃IDC) organic ligands to construct four solvent-induced POMs-Ln-organic 3D compounds by one-pot solvothermal method. Especially, 1D channels along *a* and *b* axes were observed for compounds **3** and **4**, which opens a new strategy for the rational design of porous POMs-Ln-organic materials. To our best knowledge, compounds **3** and **4** for the first time represent 3D inorganic-organic framework based on lanthanide, Keggin-POMs and 4,5-imidazole dicarboxylic acid. In addition, we highlight an available method to successfully fabricate POMs 3D framework anchoring Ag nanocomposites by simultaneous reduction and stabilization effect of reduced POMs and ultra-violet light. Furthermore, we demonstrated the catalytic study of the as-prepared composites towards the reduction of 4-NP by the assistance of NaBH₄.

Experimental

Materials and methods

All the reagents were commercially purchased and used without further purification. LaCl₃·6H₂O and CeCl₃·6H₂O were commercially purchased from Beijing HWRK Chem. Co., Ltd. with purity of 99.99%. AgNO₃ and NaBH₄ were purchased from Aladdin company. The precursor K₈[SiW₁₁O₃₉]·13H₂O was synthesized according to the literature method.³⁷ Elemental analyses were performed for C, H, and N on a Perkin-Elmer 2400 CHN elemental analyzer; for W and Ln on a Leaman inductively coupled plasma (ICP) spectrometer. IR spectra were recorded in the 400–4000 cm⁻¹ region on an Alpha Centaur FT/IR spectrophotometer (KBr pellets). TG analyses were performed on a SDT Q600 V20.9 Build 20 Perkin-Elmer TGA7 instrument under N₂ atmosphere with a heating rate of 5 °C min⁻¹. XPRD (X-ray Powder Diffraction) of samples were recorded with a Rigaku D/max-III-B diffractometer (Tokyo, Japan) with Cu Kα irradiation (λ = 1.54178 Å). Hydrothermal syntheses were carried out in 15 mL Teflon-lined reactor under autogenous pressure. SEM observations were performed on a FEI Quanta 200 scanning electron microscope. The acceleration voltage was set to 10 kV. The sample was stuck on the observation platform and sprayed with gold vapor under high vacuum for about 60 s. TEM was performed using a field emission TecnaiG2F30 (FEI, US). The EDS was coupled with SEM and measured at 20 kV.

General procedure for synthesis of K₄La₃(HIDC)₃(IDC)₃(H₂O)₃(SiW₁₂O₄₀)·7H₂O (1). A mixture of LaCl₃·7H₂O (0.8 mmol, 0.2826 g), K₈[SiW₁₁O₃₉]·13H₂O (0.4 mmol, 1.2880 g), H₃IDC (0.6 mmol, 0.0936 g), were added to 10 mL of a CH₃CH₂OH/H₂O mixture (6/4, v/v), magnetically stirring for 1 h at room temperature, then sealed in a 15 mL Teflon-lined reactor and kept at 140 °C for 5 days. The reactor was then slowly cooled down to room temperature over a period of 9 h. Yellow block crystals were filtered, washed with distilled water and dried at 80 °C. Yield: 29% (based on W). Anal. Calcd for **1**: W, 48.43; La, 9.14; K, 3.43; C, 7.91; H, 0.77; N, 3.69 (%). Found: W, 47.79; La, 8.92; K, 3.35; C, 7.71; H, 1.21; N, 3.85 (%). FTIR (KBr): 3374s, 1560m, 1557s, 1509m, 1493m, 1450m, 1424m, 1375s, 1250w, 1227w, 1126w, 1018w, 967m, 922s, 880m, 807s, 791s, 777s, 657m, 628m, 538m, 517m cm⁻¹. The TG curve of **1** exhibits a two-step continuous weight loss process: the weight loss of 3.42% (calcd 3.58%) from 25

to 163 °C corresponds to the loss of all lattice water and coordinated water molecules. The weight loss of 17.61% (calcd 17.29%) from 163 to 556 °C corresponds to the decomposition of organic ligands and formation of oxycarbonate La₂O₂(CO₃).³⁸

General procedure for synthesis of K₄Ce₃(HIDC)₃(IDC)₃(H₂O)₃(SiW₁₂O₄₀)·6H₂O (2). The synthetic procedure was prepared in the same way as **1**, except using CeCl₃·7H₂O to replace LaCl₃·7H₂O. Yellow block crystals were obtained. Yield: 30% (based on W). Anal. Calcd for **2**: W, 48.59; Ce, 9.26; K, 3.44; C, 7.94; H, 0.73; N, 3.70 (%). Found: W, 48.35; Ce, 9.05; K, 3.61; C, 7.79; H, 0.82; N, 3.88 (%). FTIR (KBr): 3370s, 1562m, 1558s, 1509m, 1492m, 1451m, 1423m, 1373s, 1248w, 1228w, 1125w, 1019w, 968m, 922s, 881m, 808s, 789s, 775s, 656m, 627m, 541m, 513m cm⁻¹. TG curve of **2** exhibits a two-step continuous weight loss process: the weight loss of 3.88% (calcd 3.96%) from 25 to 161 °C corresponds to the loss of all lattice water and coordinated water molecules. The weight loss of 17.66% (calcd 17.21%) from 161 to 550 °C corresponds to the decomposition of organic ligands and formation of oxycarbonate La₂O₂(CO₃).³⁸

General procedure for synthesis of La₄(HIDC)₄(SiW₁₂O₄₀)(8H₂O)·11H₂O (3). A mixture of LaCl₃·7H₂O (0.8 mmol, 0.2826 g), K₈[SiW₁₁O₃₉]·13H₂O (0.4 mmol, 1.2880 g), H₃IDC (0.6 mmol, 0.0936 g), were added to 10 mL of a CH₃CH₂OH/H₂O mixture (4/6, v/v), magnetically stirring for 1 h at room temperature, then sealed in a 15 mL Teflon-lined reactor and kept at 140 °C for 5 days. The reactor was then slowly cooled down to room temperature over a period of 9 h. Yellow block crystals were filtered, washed with distilled water and dried at 80 °C. Yield: 25% (based on W). Anal. Calcd for **3**: W, 50.27; La, 12.66; C, 5.47; H, 1.06; N, 2.55 (%). Found: W, 49.98; La, 12.47; C, 5.21; H, 1.26; N, 2.71 (%). FTIR (KBr): 3428s, 1563m, 1543m, 1496m, 1385m, 1244w, 1093w, 1038w, 1019w, 971m, 921s, 883w, 804s, 657w, 532w cm⁻¹. TG curve of **3** exhibits a two-step continuous weight loss process: the weight loss of 7.93% (calcd 7.80%) from 25 to 176 °C corresponds to the loss of all lattice water and coordinated water molecules. The weight loss of 9.93% (calcd 9.85%) from 176 to 560 °C corresponds to the decomposition of the HIDC ligands and formation of oxycarbonate La₂O₂(CO₃).³⁸

General procedure for synthesis of Ce₄(HIDC)₄(SiW₁₂O₄₀)(8H₂O)·11H₂O (4). The synthetic procedure was prepared in the same way as **3**, except using CeCl₃·7H₂O to replace LaCl₃·7H₂O. Yellow block crystals were obtained. Yield: 25% (based on W). Anal. Calcd for **4**: W, 50.22; Ce, 12.76; C, 5.47; H, 1.06; N, 2.55 (%). Found: W, 49.92; Ce, 12.57; C, 5.23; H, 1.26; N, 2.68 (%). FTIR (KBr): 3426s, 1563m, 1543m, 1495m, 1387m, 1241w, 1092w, 1038w, 1018w, 970m, 921s, 884w, 805s, 658w, 535w cm⁻¹. TG curve of **4** exhibits a two-step continuous weight loss process: the weight loss of 7.69% (calcd 7.79%) from 25 to 176 °C corresponds to the loss of all lattice water and coordinated water molecules. The weight loss of 9.85% (calcd 9.23%) from 176 to 560 °C corresponds to the decomposition of the HIDC ligands and formation of oxycarbonate La₂O₂(CO₃).³⁸

General procedure for preparation of Ag@Crystals nanocomposites. Freshly ground **1** (7 mg) were dispersed in 3 mL distilled water containing 1 mg AgNO₃ and 200 μL ethylene glycol at room temperature. The mixture was irradiated under 125 W ultra-violet lamp at 15 cm distance for 1.5 h. Then Ag@**1** was centrifuged at 12000 rpm, rinsed triply by distilled water. The as-prepared composites were stored in 2 mL distilled water, and placed in dark room for further use. Other crystals and (TBA)₄SiW₁₂O₄₀ supporting Ag nanocomposites were prepared in a similar way.

General procedure for the reduction of 4-NP. 1 mL of 0.01 mol·L⁻¹ 4-NP was added to 1 mL 3.8 mg/mL NaBH₄ aqueous

Table 1 Crystal Data and Structure Refinement for Compounds 1 to 4.

Complex	1	2	3	4
Empirical formula	C ₃₀ H ₃₅ K ₄ La ₃ N ₁₂ O ₇₄ SiW ₁₂	C ₃₀ H ₃₃ K ₄ Ce ₃ N ₁₂ O ₇₃ SiW ₁₂	C ₂₀ H ₄₆ La ₄ N ₈ O ₇₅ SiW ₁₂	C ₂₀ H ₄₆ Ce ₄ N ₈ O ₇₅ SiW ₁₂
Formula weight	4554.91	4540.53	4388.38	4393.22
Temperature	296(2) K	296(2) K	293(2) K	293(2) K
Wavelength	0.71073 Å	0.71073 Å	0.71073 Å	0.71073 Å
Crystal system	Rhombohedral	Rhombohedral	Monoclinic	Monoclinic
space group	$R\bar{3}$	$R\bar{3}$	$P2(1)/c$	$P2(1)/c$
a (Å)	22.0842(2)	22.1520(4)	13.685(5)	13.7014(10)
b (Å)	22.0842(2)	22.1520(4)	13.144(4)	13.1554(10)
c (Å)	28.0921(6)	28.2012(12)	22.649(7)	22.7273(17)
α (°)	90°	90°	90°	90°
β (°)	90°	90°	100.551(5)°	100.3360(10)°
γ (°)	120°	120°	90°	90°
V (Å ³)	11865.3(3)	11984.6(6)	4005(2)	4029.7(5)
Z	6	6	2	2
D_c (Mg m ⁻³)	3.824	3.774	3.639	3.620
M (mm ⁻¹)	19.304	19.219	19.370	19.398
F (000)	11902	11968	3796	3884
Limiting indices	-24 ≤ h ≤ 21 -23 ≤ k ≤ 24 31 ≤ l ≤ 22	-27 ≤ h ≤ 7 -27 ≤ k ≤ 27 -34 ≤ l ≤ 34	-16 ≤ h ≤ 16 -10 ≤ k ≤ 16 -27 ≤ l ≤ 27	-16 ≤ h ≤ 16 -13 ≤ k ≤ 16 -28 ≤ l ≤ 27
Measured reflections	16772	90136	20041	21194
Independent reflections	3855	5214	7563	7821
$R_{(int)}$	0.0436	0.0658	0.1231	0.0344
Data/restraints/parameters	3855 / 0 / 397	5214 / 0 / 401	7563 / 6 / 365	7821 / 6 / 438
Goodness-of-fit on F^2	1.011	1.012	1.010	1.014
$R_1,^a wR_2^b [I > 2\sigma(I)]$	0.0327, 0.0716	0.0227, 0.0513	0.0838, 0.1734	0.0730, 0.1487
$R_1,^a wR_2^b$ (all data)	0.0438, 0.0763	0.0269, 0.0533	0.1585, 0.2035	0.0782, 0.1514

$$^a R_1 = \frac{\sum |F_o| - |F_c|}{\sum |F_o|}; \quad ^b wR_2 = \left\{ \frac{\sum [w(F_o^2 - F_c^2)^2]}{\sum [w(F_o^2)^2]} \right\}^{1/2}$$

solution. Subsequently, 50 μ L 7 mg/mL composites aqueous dispersions (Ag@Crystals) was added. After addition of Ag@Crystals, the characteristic absorption peak of 4-nitrophenolate ion at 400 nm gradually decreased. Simultaneously, a new peak at \sim 300 nm, ascribable to newly generated 4-AP, emerged. The peak of 4-nitrophenolate ions at 400 nm completely disappeared in 60 to 120 seconds for different composites. The absorption spectra of the solution were recorded in the range of 250-500 nm. The rate constants of the reduction process (k_{app}) were determined using the following equations: $-dC_t/dt = kC_t$ and $\ln(C_t/C_0) = -kt$. The reduction reaction of 4-NP with NaBH₄ in the absence of composites has also been carried out under similar condition.

Crystallographic data collection and refinement X-ray single crystal diffraction data for compounds 1 to 4 were collected on a Bruker Apex-II CCD detector using graphite monochromatized Mo $K\alpha$ radiation ($\lambda = 0.71073$ Å) at room temperature. Routine Lorentz and polarization corrections were applied. The structures were solved by direct methods and refined on F^2 by full-matrix least squares using the SHELXTL-97 program package on a legend computer.^{39, 40} All of the non-hydrogen atoms except some disordered atoms were refined with anisotropic thermal displacement coefficients. Hydrogen atoms in IDC ligands were assigned to calculated positions using a riding model with appropriately fixed isotropic thermal parameters. Si (for 3) and W4 (for 4) atoms were refined by ISOR order to avoid non-positive-definite result. The detailed crystallographic data and structure refinement parameters are summarized in Table 1. Selected bond distances for compounds

1 to 4 are listed in Tables S1 to S4. These four compounds for the structures reported in this paper have been deposited in the Cambridge Crystallographic Data Center with CCDC numbers 828025 for 1, 828026 for 2, 936028 for 3, 936029 for 4.

Results and discussion

Synthesis

In the syntheses of 1 to 4, solvent plays a key role in the formation of final products. In our initial experiments, compound 3 or 4 were designed to be synthesized under hydrothermal conditions. However, only light yellow powders can be obtained. When solvent was replaced by the mixture of water and ethanol, the yields of 3 or 4 increased with the increasing ratio of water and ethanol. At the ratio of ca. 6:4, the yields of crystalline 3 or 4 reaches the highest value of ca. 25%. At this ratio, small amount of compound 1 or 2 began to form as byproduct. By increasing the proportion of ethanol in the solvent, compound 1 or 2 can be obtained as main products in a highest yield of 30% at the ratio of 4:6 for water/ethanol. We assumed that the ion pairing of potassium and carboxylate in IDC will be strengthened by the higher content of ethanol during hydrothermal process due to the better solubility of IDC in ethanol, which might result in the introduction of K⁺ and isolated IDC ligands inside the crystals.⁴¹ Furthermore, the higher ratio for water/ethanol will lead to unidentified powders.

Thus, the syntheses of **1** to **4** can be considered as solvent-controlled process, in which the products can be modulated by different component ratio of mixed solvent. In addition, the POM precursor is monovacant Keggin-POM $[\text{SiW}_{11}\text{O}_{40}]^{10-}$, while the saturated Keggin-POM $[\text{SiW}_{12}\text{O}_{40}]^{4-}$ was isolated in the final product, suggesting a structure transformation during the reaction process. This phenomenon is in agreement with the former reported compounds.⁴²

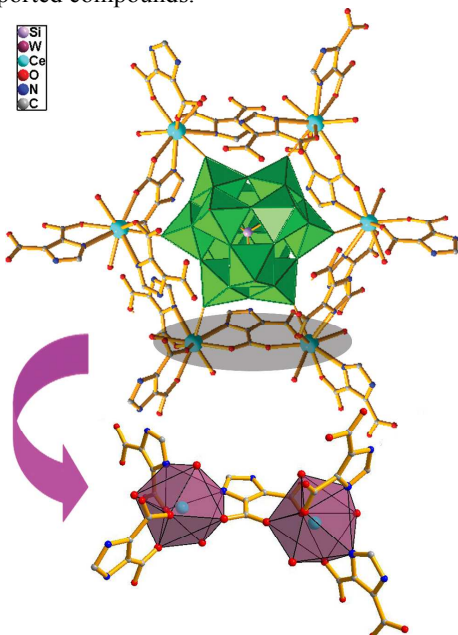


Fig. 1 Combined polyhedral and ball-stick representation of the molecular structure unit of **2** (top). The two polyhedrons represent the Ce^{3+} coordinate modes (bottom). All the hydrogen atoms and water molecules have been omitted for clarity.

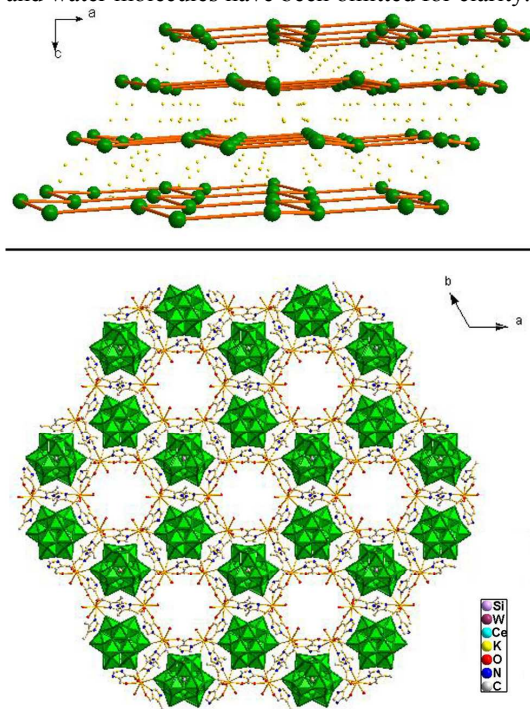


Fig. 2 Ball-stick representation of compound **2** (polyoxoanion is denoted as big green ball) along *b* axes (top). Polyhedron and ball-stick view of the 2D sheet structure of **2** along *c* axes (bottom).

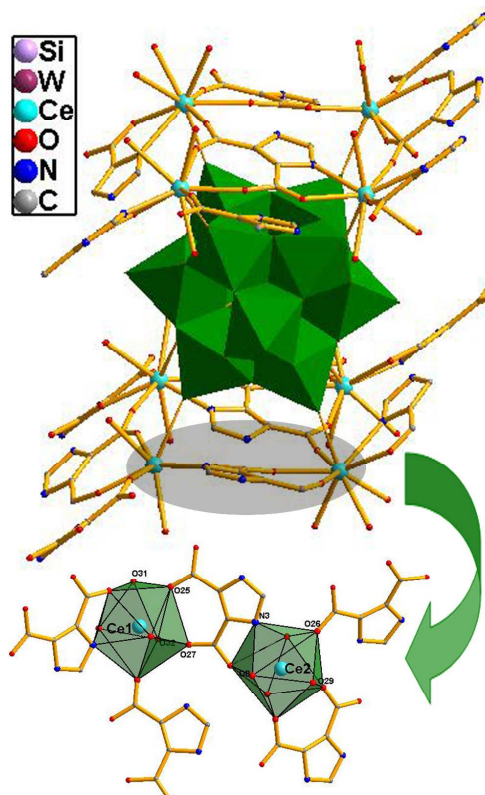


Fig. 3 Combined polyhedral and ball-stick representation of the molecular structure unit of **4** (top). All the hydrogen atoms and water molecules have been omitted for clarity.

Structural descriptions

Single crystal X-ray diffraction analyses reveal that compounds **1** and **2** are isomorphous POM-Ln-organic hybrids, of which the unit cell dimensions, volumes, related bond distances and angles are only slightly changed. Thus, we discuss the structure of **2** in detail as a typical example. Compound **2** is made up of one $[\text{SiW}_{12}\text{O}_{40}]^{4-}$, three Ce^{3+} ions, three H_2IDC and three HIDC ligands, four K^+ and seven water molecules, in which Si atom lies on a three-fold axis. The inorganic $[\text{SiW}_{12}\text{O}_{40}]^{4-}$ polyoxoanion exhibits a typical α -Keggin structure. The central atom Si is disorderly surrounded by a cube of eight oxygen atoms, with each oxygen site half-occupied, as has been observed in previous literatures.⁴³ As shown in Fig. 1, each Ce^{3+} ion coordinates to three nitrogen and three oxygen atoms arising from organic ligands, while the other two positions are occupied by one coordinated water molecule and one oxygen atom from another polyoxoanion. Coordination geometry of each Ce^{3+} can be viewed as tricapped triangular prism as common coordination style for Ln complexes. Interestingly, three coordinated imidazole ligands for each Ce^{3+} present unusual mutually perpendicular conformation for imidazole planes. The dihedral angles for each pair of imidazole planes are 86.6° , 87.2° and 87.5° respectively, indicating an almost perpendicular mode. This kind of coordination mode is firstly observed for ligand geometry in POM-Ln-organic complexes. The coordination style of Ce^{3+} and imidazole ligands propagates along *ab* plane and thus forming a hexameric Ln_6 cycles. By linkage of Ln ions among neighboring polyoxoanions, compound **1** or **2** forms 2D honeycomb Ln-organic hexagon grids along *ab* plane. Neighboring 2D layers arrange each other in staggered pattern, which are further

constructed by K^+ cations to generate the solid with the features of a six-connected node and coordinates to six Ce^{3+} ions through terminal oxygen atoms from POMs. The Ce–O distances are in the range of 2.461(5)–2.650(4) Å. The K^+ cations are mainly located in the cavities formed by enclosure of six Ce_6 units (Fig. 2). Along c axis, compound **1** or **2** can be viewed as the assembly of K^+ cationic and POM-Ln-Organic anionic layers alternately.

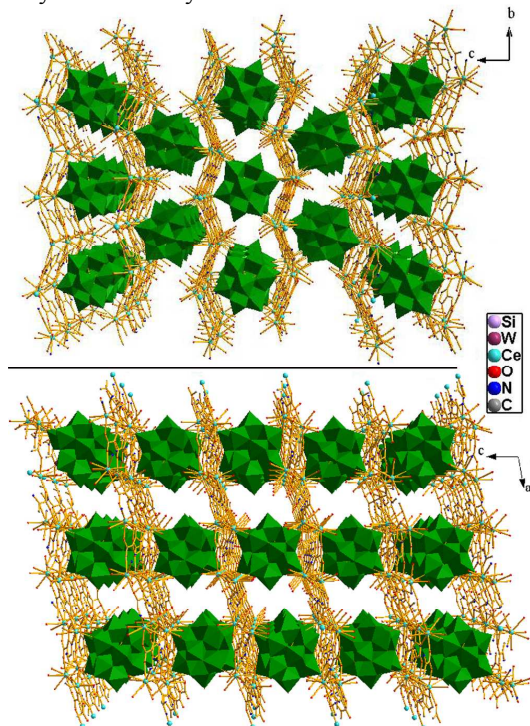


Fig. 4 Polyhedron and ball-stick view of the 3D architecture of **4** along a axes (top) and b axes (bottom).

Compounds **3** and **4** are also isomorphous, thus, we continue to discuss the structure of **4** as an example. Complex **4** contains $[SiW_{12}O_{40}]^{4-}$ polyoxoanions, Ce^{3+} cations, HIDC ligands, coordinated and isolated water molecules, in which the Si atom lies on an inversion centre in each case, with concomitant disorder of the oxygen atoms bonded to the Si atom. Two crystallographically independent Ce^{3+} cations are both nine-coordinated by one or two carboxyl oxygen atoms from two H_3IDC ligands, one carboxyl oxygen atom and one nitrogen atom from another HIDC ligand, two oxygen atoms from different polyoxoanions, and two oxygen atoms from coordinated water molecules (Fig. 3). Similar to compound **1** or **2**, Ce(1) ion in **3** or **4** is nine-coordinated in a tricapped triangular prism geometry. Ce(2) ion is also nine coordinated, however, the minimum dihedral angle of 4.2° between two edge sharing triangles is smaller than that of Ce(1) as 11.6° . These two values are both smaller than that of Ln ion in compound **1** or **2** as 15.5° , suggesting that Ce ions in compound **4** present an intermediate state between tricapped triangular prism and monocapped triangular antiprism. The coordination mode between Ce and HIDC ligands propagate along ab plane and thus forming a 2D layered structure. These undulated 2D layers are further connected by polyoxoanion pillars to construct 3D architectures. Interestingly, along a or b axis, neighboring polyoxoanion chains and Ce-organic layers enclose one dimensional channels (Fig. 4). To the best of our knowledge, this is the first example of 3D Keggin type

polyoxometalate induced POM-Ln-organic compounds with 1D channels. The accessible void volumes of the channels in **3** or **4** are 25.5% and 25.7% of the unit cell volumes. In the 3D structure, each $[SiW_{12}O_{40}]^{4-}$ anion connect eight Ce ions by covalent Ce–O bonds, of which the distances are in the range of 2.418(15)–2.802(17) Å. By a topology analysis, each $[SiW_{12}O_{40}]^{4-}$ anion can be viewed as eight connected node, which directly link eight Ce ions. Further, if HIDC ligand and Ce ion are considered as three-connected and five-connected coordination node respectively, 3D architecture of compound **3** or **4** forms a 3,3,5,5,8-connected net with a point symbol of $\{4.6^2\}_2\{4^{10}.6^2.8^{12}.10^4\}\{4^3\}_2\{4^4.6^5.8\}_2\{4^5.6^5\}_2$ (Fig. S12). As compared to the reported POM-Ln-organic compounds, Keggin type $[SiW_{12}O_{40}]^{4-}$ anion in compound **3** or **4** firstly act as eight-connected linker to coordinate to the surrounding Ln ions covalently by elaborate selection of N-heterocycle carboxylic acid ligand, which paves the way to design variety of 3D POM-Ln-organic compounds. Taken together, compounds **1** and **2** represent the 3D supramolecular architectures including 2D layered structures connected by K^+ cations. However, compound **3** and **4** composed of 2D Ln-organic networks and polyoxoanions pillars, possess 3D covalent frameworks featuring with 1D channels.

Reduction of 4-NP

Considering the 3D framework of as-synthesized crystals, it is speculated that compounds **1** to **4** might be an ideal matrix or supports for the nucleation and growth of silver nanocomposites. As above mentioned, reduced POMs could spontaneously generated noble metals nanostructures due to their superior redox properties. Therefore, we tend to use the synergistic effect of reduced POMs and ultra-violet light to generate silver nanostructures. It is worth mentioning that POMs could also play stabilizing role during the growth of silver nanostructure, as proved previously. Scanning electron microscopy (SEM) images of ground crystals for the convenience of running catalytic reaction are shown in Fig. 5a, b, c, and d. The lateral sizes of irregular particles are ranging from 1 to 15 μm . In the cases of **1** and **2**, silver nanowires are unexpectedly generated after soaking the ground powder in $AgNO_3$ aqueous solution under the irradiation of UV light for 1.5 h, as seen in Fig 5e and f. We assumed that the nucleation occurred in the cavity of the framework, while the continuance of growing process caused the collapse of crystal structure due to its dynamically non-covalent linkage. The slow growth rate and induction by the cavity of structures ensured the formation of one-dimensional silver nanowires. In contrast, as illustrated in Fig. 5g and h, silver nanoparticles were clearly observed on the surface of crystals **3** and **4**. The crystal structures almost remained after treatment by similar irradiation condition. The morphology of silver nanoparticles might be ascribed to the strong confinement effect of porous structures in crystals **3** and **4**, which were constructed by stable covalent linkage. As depicted in Fig. 5d, h, l, and p, Energy dispersive spectroscopy (EDS) analysis confirmed the existence of Ag element evenly distributed along composites. The representative transmission electron microscopy (TEM) images of silver nanostructures corresponding to **1** to **4** crystals are illustrated in Fig. 5 c, g, k, and o. Nanowires and nanoparticles Ag nanostructures are clear to see for respective $Ag@1$, $Ag@2$, $Ag@3$, and $Ag@4$. The nanowire is *ca.* 10 nm in diameter, and dozens of micrometers in length. The fibers with bundle structures are composed of hundreds of individual nanowires. The nanoparticles were around 12 nm in lateral sizes.

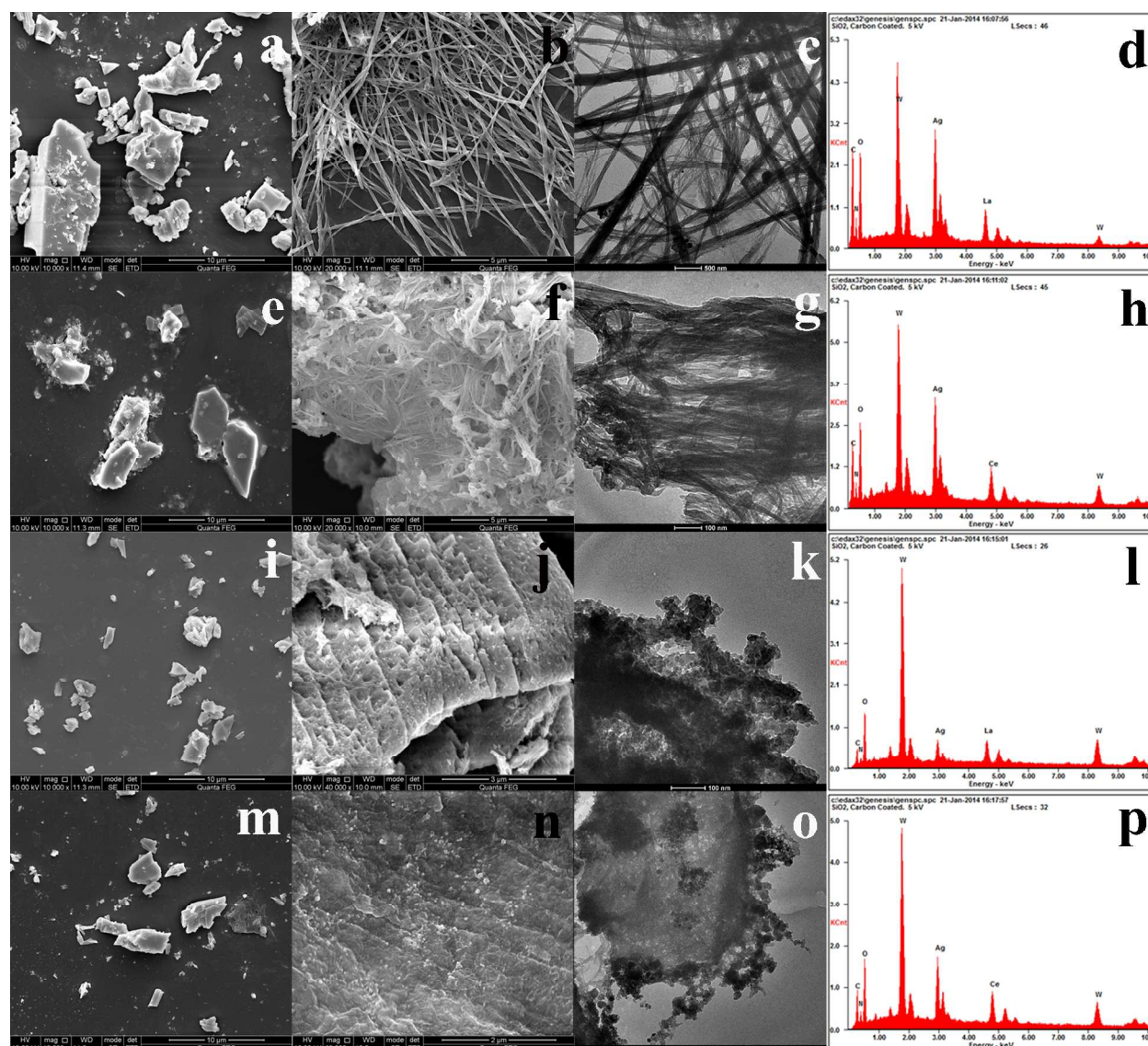


Fig. 5 (a) and (e) are SEM images of ground crystals **1** and **3**; (b) and (f) are SEM images of Ag@**1** and Ag@**3** nanocomposites, and (c) and (g) are corresponding TEM images; (d) and (h) are EDS of representative Ag@**1** and Ag@**3** nanocomposites. EDS are coupled with SEM equipment, and measured for three times to check out the consistency.

Subsequently, we selected the reduction of 4-NP by excess NaBH_4 as a model reaction to test the catalytic activity of Ag@Crystals.⁴⁴ Generally, the reaction was performed under ambient conditions. The 4-NP solution gave a strong absorption peak at 317 nm in neutral or acidic conditions. Upon the addition of NaBH_4 solution, the position of characteristic peak of 4-NP shifted from 317 to 400 nm immediately because of the formation of 4-nitrophenolate ion, accompanying the color change of light yellow to yellow-green.^{45, 46} After the addition of Ag@**1**, the color of the 4-nitrophenolate ions was invisible after 90 s, which was recorded by UV-vis spectroscopy. As shown in Fig. 6a, the characteristic absorption peak of 4-nitrophenolate ion at 400 nm gradually decreased, while new peak of 4-AP appeared at 295 nm. The addition of other Ag@Crystals catalysts, the reduction reactions complete in 60 to 120 s under similar conditions. In order to check out the catalytic nature of catalyst, the reduction reaction of 4-NP in the absence of Ag@Crystals was carried out. It is obvious to

see that the 4-NP characteristic peak intensity at 400 nm was almost constant in 10 min (Fig. S13).

In order to get the apparent kinetic rate constant K_{app} , $\ln(C_t/C_0)$ and C_t/C_0 versus reaction time for the reduction of 4-NP over different Ag@Crystals nanocomposite were plotted in Fig. 6. It could be observed that the kinetic constants K_{app} was 4.75×10^{-2} , 4.4×10^{-2} , 3.62×10^{-2} , and 6.65×10^{-2} corresponding to Ag@**1**, Ag@**2**, Ag@**3**, and Ag@**4**, respectively. It is worth mentioning that these K_{app} constants were much higher than other catalytic systems related to POM supported noble metal particles.⁹ The superior advantages of present systems are three folds: (1) the 3D framework provides ideal growing place for the preparation of metal nanostructures; (2) the intrinsic redox properties of POMs would facilitate the formation of metal nanostructures spontaneously by the assistance of UV light; (3) the small diameter of Ag nanowires and lateral sizes of Ag nanoparticles lead to large surface area, thus enhance the contacting opportunity with 4-NP, which would eventually resulted in the high catalytic activity. Additionally, as shown in Fig. S12, the

control experiment of $(\text{TBA})_4\text{SiW}_{12}\text{O}_{40}$ as support for anchoring Ag was performed to check the superiority of 3D porous structures. Obviously, the yellow-green color was unchanged in 10 min due to the extreme lower loading of Ag nanostructures on the surface of $(\text{TBA})_4\text{SiW}_{12}\text{O}_{40}$. EDS data also confirmed that the Ag loading are very low, because the content might be below or at least close to the detection limit of EDS, which can be seen in Figure S13. Our preliminary data clearly showed that 3D framework consisting of POMs were good candidates for anchoring AgNPs because of their porosity, redox, and diversity.

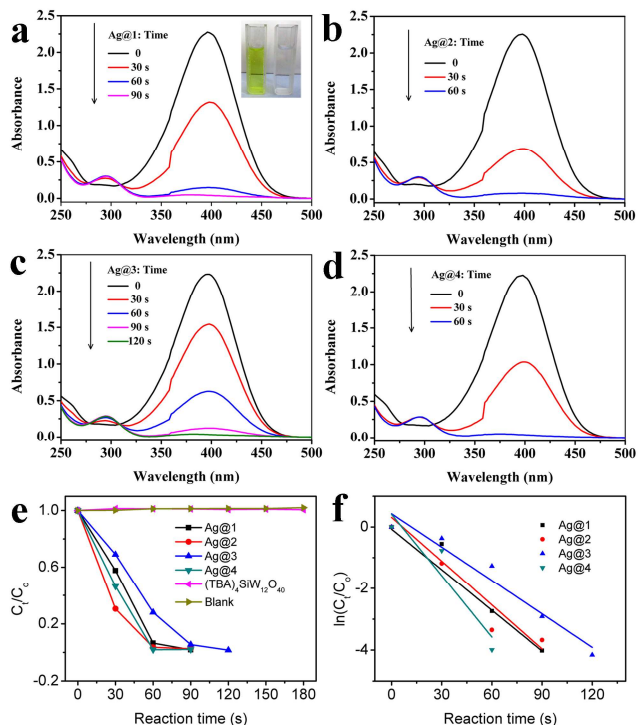


Fig. 6 (a), (b), (c), and (d) are absorption spectra of 4-nitrophenolate ion in distilled water during the reduction reaction in the presence of NaBH_4 with the catalysts of Ag@1, Ag@2, Ag@3, and Ag@4, respectively. The inset in panel (a) is the digital image of reaction solution before and after reduction. (e) are the plots of C_t/C_0 versus reaction time in different catalytic system, in which C_t is the 4-nitrophenolate ion concentration at reaction time t and C_0 is the initial concentration. (f) are plotted by $\ln(C_t/C_0)$ versus reaction time. The apparent reaction rate constants were acquired after linear fitting.

Conclusions

In summary, 3D POM-Ln-organic compounds **1** to **4** have been successfully isolated under solvothermal conditions. It has been concluded that the ratio of water and ethanol plays an important role in forming the final products. Especially, the formation of compound **3** or **4** opens a new way for the rational design of 3D POM-Ln-organic compounds by modulating solvent ratio, in which the increase of ethanol in reaction system inhibits the formation of K^+ ions in the final crystalline product. Our results further confirmed that these 3D POM-Ln-organic compounds could successfully generate Ag nanocomposites, which possessed good catalytic activity for the reduction of 4-NP to 4-AP by the assistance of NaBH_4 . The control experiments

showed that the redox properties and the diversity of structures play vital role in enhancing the catalytic efficiency significantly.

Acknowledgements

We thank the National Natural Science Foundation of China (Grant No. 21271034 and 21103035), Heilongjiang Province Natural Science Funds for Distinguished Young Scholar (No. JC201220), Natural Science Foundation of Heilongjiang Province (No. QC2011C038), Heilongjiang Universities' Science and Technology Innovation Team program (2012TD010). And the Fundamental Research Funds for the Central Universities (Grant No. HIT. NSRIF. 2011025), SKLUWRE (QA201022). We also thank Prof. Shuang-Quan Zang from Zhengzhou University for the help of X-ray single crystal determination.

Notes and references

^a Department of Chemistry, College of Pharmacy, Jiamusi University, Jiamusi 154004, China.

^b State Key Lab of Urban Water Resource and Environment (SKLUWRE) & Academy of Fundamental and Interdisciplinary Science, Harbin Institute of Technology, Harbin, Heilongjiang, 150080, China.

^c Department of Chemistry, Changchun Normal University, Changchun 130032, China.

† Electronic Supplementary Information (ESI) available: IR, XRD, TGA, UV-vis, SEM, EDS, and CIF files. See DOI: 10.1039/b000000x/

- M. T. Pope, *Heteropoly and Isopoly Oxometalates*, Springer, Berlin, 1983.
- X. Fang, P. Kogerler, M. Speldrich, H. Schilder and M. Luban, *Chem. Soc. Rev.*, 2012, **48**, 1218–1220.
- Z. M. Zhang, Y. G. Li, S. Yao, E. B. Wang, Y. H. Wang and R. Clérac, *Angew. Chem., Int. Ed.*, 2009, **121**, 1609–1612.
- A. Proust, B. Matt, R. Villanneau, G. Guillemot, P. Gouzerh and G. Izzet, *Chem. Soc. Rev.*, 2012, **41**, 7605–7622.
- Y. Bai, G. Q. Zhang, D. B. Dang, P. T. Ma, H. Gao and J. Y. Niu, *CrystEngComm*, 2011, **13**, 4181–4187.
- X. Feng, W. Zhou, Y. Li, H. Ke, J. Tang, R. Clérac, Y. Wang, Z. Su and E. Wang, *Inorg. Chem.*, 2012, **51**, 2722–2724.
- Y. Kikukawa, Y. Kuroda, K. Yamaguchi and N. Mizuno, *Angew. Chem., Int. Ed.*, 2012, **51**, 2434–2437.
- Q. Yin, J. M. Tan, C. Besson, Y. V. Geletii, D. G. Musaev, A. E. Kuznetsov, Z. Luo, K. I. Hardcastle and C. L. Hill, *Science*, 2010, **328**, 342–345.
- D. Y. Du, J. S. Qin, T. T. Wang, S. L. Li, Z. M. Su, K. Z. Shao, Y. Q. Lan, X. L. Wang and E. B. Wang, *Chem. Sci.*, 2012, **3**, 705–710.
- C. Ritchie, V. Baslon, E. G. Moore, C. Reber and C. Boskovic, *Inorg. Chem.*, 2011, **51**, 1142–1151.
- D. Y. Du, L. K. Yan, Z. M. Su, S. L. Li, Y. Q. Lan and E. B. Wang, *Coord. Chem. Rev.*, 2013, **257**, 702–717.
- F. J. Ma, S. X. Liu, C. Y. Sun, D. D. Liang, G. J. Ren, F. Wei, Y. G. Chen and Z. M. Su, *J. Am. Chem. Soc.*, 2011, **133**, 4178–4181.

13. J. Song, Z. Luo, D. K. Britt, H. Furukawa, O. M. Yaghi, K. I. Hardcastle and C. L. Hill, *J. Am. Chem. Soc.*, 2011, **133**, 16839–16846.
14. Y. Zhu, P. Yin, F. Xiao, D. Li, E. Bitterlich, Z. Xiao, J. Zhang, J. Hao, T. Liu, Y. Wang and Y. Wei, *J. Am. Chem. Soc.*, 2013, **135**, 17155–17160.
15. S. Li, S. Liu, S. Liu, Y. Liu, Q. Tang, Z. Shi, S. Ouyang and J. Ye, *J. Am. Chem. Soc.*, 2012, **134**, 19716–19721.
16. H. Fu, C. Qin, Y. Lu, Z. M. Zhang, Y. G. Li, Z. M. Su, W. L. Li and E. B. Wang, *Angew. Chem., Int. Ed.*, 2012, **51**, 7985–7989.
17. Y. P. Xie and T. C. W. Mak, *Angew. Chem., Int. Ed.*, 2012, **51**, 8783–8786.
18. C. Y. Sun, S. X. Liu, D. D. Liang, K. Z. Shao, Y. H. Ren and Z. M. Su, *J. Am. Chem. Soc.*, 2009, **131**, 1883–1888.
19. B. S. Bassil, M. H. Dickman, I. Römer, B. von der Kammer and U. Kortz, *Angew. Chem., Int. Ed.*, 2007, **46**, 6192–6195.
20. T. Yamase, *Chem. Rev.*, 1998, **98**, 307–326.
21. R. C. Howell, F. G. Perez, S. Jain, J. W. DeW. Horrocks, A. L. Rheingold and L. C. Francesconi, *Angew. Chem., Int. Ed.*, 2001, **40**, 4031–4034.
22. W. Xu, Q. Luo, H. Wang, L. C. Francesconi, R. E. Stark and D. L. Akins, *J. Phys. Chem. B*, 2003, **107**, 497–501.
23. O. Dmitrenko, W. Huang, T. E. Polenova, L. C. Francesconi, J. A. Wingrave and A. V. Teplyakov, *J. Phys. Chem. B*, 2003, **107**, 7747–7752.
24. S. Li, D. Zhang, Y. Y. Guo, P. Ma, X. Qiu, J. Wang and J. Niu, *Dalton Trans.*, 2012, **41**, 9885–9888.
25. Y. Gao, Y. Xu, Z. Han, C. Li, F. Cui, Y. Chi and C. Hu, *J. Solid State Chem.*, 2010, **183**, 1000–1006.
26. H. An, H. Zhang, Z. Chen, Y. Li, X. Liu and H. Chen, *Dalton Trans.*, 2012, **41**, 8390–8400.
27. K. Wang, D. Zhang, J. Ma, P. Ma, J. Niu and J. Wang, *CrystEngComm*, 2012, **14**, 3205–3212.
28. D. D. Liu and Y. G. Chen, *Inorg. Chim. Acta* 2013, **401**, 70–75.
29. C. Qin, X. Z. Song, S. Q. Su, S. Dang, J. Feng, S. Y. Song, Z. M. Hao and H. J. Zhang, *Dalton Trans.*, 2012, **41**, 2399–2407.
30. J. Geng, M. Li, J. Ren, E. Wang and X. Qu, *Angew. Chem., Int. Ed.*, 2011, **123**, 4270–4274.
31. P. Yin, J. Wang, Z. Xiao, P. Wu, Y. Wei and T. Liu, *Chem. Eur. J.*, 2012, **18**, 9174–9178.
32. Z. Ma, Q. Liu, Z. M. Cui, S. W. Bian and W. G. Song, *J. Phys. Chem. C*, 2008, **112**, 8875–8880.
33. N. Mizuno and K. Kamata, *Coord. Chem. Rev.*, 2011, **255**, 2358–2370.
34. P. J. Kulesza, M. Chojak, K. Karnicka, K. Miecznikowski, B. Palys, A. Lewera and A. Wieckowski, *Chem. Mater.*, 2004, **16**, 4128–4134.
35. A. Troupis, A. Hiskia and E. Papaconstantinou, *Angew. Chem., Int. Ed.*, 2002, **41**, 1911–1914.
36. G. Zhang, B. Keita, R. N. Biboum, F. Miserque, P. Berthet, A. Dolbecq, P. Mialane, L. Catala and L. Nadjo, *J. Mater. Chem.*, 2009, **19**, 8639–8644.
37. A. Tézé and G. Hervé, *John Wiley and Sons, New York*, 1990.
38. M. X. Hu, Y. G. Chen, C. J. Zhang and Q. J. Kong, *CrystEngComm*, 2010, **12**, 1454–1460.
39. G. M. Sheldrick, *SHELXS-97, Program for Crystal Structure Solution, University of Göttingen, Germany*, 1997.
40. G. M. Sheldrick, *SHELX-97, Program for Crystal Structure Refinement, University of Göttingen, Germany*, 1997.
41. E. F. Aziz, N. Ottosson, S. Eisebitt, W. Eberhardt, B. Jagoda-Cwiklik, R. Vácha, P. Jungwirth and B. Winter, *J. Phys. Chem. B*, 2008, **112**, 12567–12570.
42. X. Liu, Y. Jia, Y. Zhang and R. Huang, *Eur. J. Inorg. Chem.*, **2010**, 4027–4033.
43. H. T. Evans and M. T. Pope, *Inorg. Chem.*, 1984, **23**, 501–504.
44. C. Yuan, W. Luo, L. Zhong, H. Deng, J. Liu, Y. Xu and L. Dai, *Angew. Chem., Int. Ed.*, 2011, **50**, 3515–3519.
45. Z. Zhang, C. Shao, P. Zou, P. Zhang, M. Zhang, J. Mu, Z. Guo, X. Li, C. Wang and Y. Liu, *Chem. Commun.*, 2011, **47**, 3906–3908.
46. S. Praharaj, S. Nath, S. K. Ghosh, S. Kundu and T. Pal, *Langmuir*, 2004, **20**, 9889–9892.

Table of contents

Solvent-controlled 3D lanthanide-polyoxometalate frameworks could reduce and stabilize the Ag nanocomposites possessing high catalytic activity towards the reduction of 4-nitrophenol.

